Measuring the orbital angular momentum of high-power laser pulses

Cite as: Phys. Plasmas **27**, 053107 (2020); https://doi.org/10.1063/5.0005140
Submitted: 24 February 2020 . Accepted: 27 April 2020 . Published Online: 19 May 2020

R. Aboushelbaya, K. Glize, A. F. Savin, M. Mayr, B. Spiers, R. Wang, N. Bourgeois, C. Spindloe, R. Bingham, and P. A. Norreys

Physics of Plasmas ARTICLE scitation.org/journal/php

Measuring the orbital angular momentum of high-power laser pulses

Cite as: Phys. Plasmas **27**, 053107 (2020); doi: 10.1063/5.0005140
Submitted: 24 February 2020 · Accepted: 27 April 2020 ·
Published Online: 19 May 2020

R. Aboushelbaya,[1,a),b)] K. Glize,[2] A. F. Savin,[1] M. Mayr,[1] B. Spiers,[1] R. Wang,[1] N. Bourgeois,[2] C. Spindloe,[3] R. Bingham,[2] and P. A. Norreys[1,2,4]

AFFILIATIONS

[1]Clarendon Laboratory, University of Oxford, Parks Road, Oxford OX1 3PU, United Kingdom
[2]Central Laser Facility, STFC Rutherford Appleton Laboratory, Didcot OX11 0QX, United Kingdom
[3]Scitech Precision Ltd., STFC Rutherford Appleton Laboratory, Didcot OX11 0QX, United Kingdom
[4]John Adams Institute for Accelerator Science, University of Oxford, Keble Road, Oxford OX1 3RH, United Kingdom

Note: This paper is part of the Special Collection: Papers from the 61st Annual Meeting of the APS Division of Plasma Physics.
Note: Paper DI3 4, Bull. Am. Phys. Soc. **64** (2019).
[a)]Invited speaker.
[b)]**Author to whom correspondence should be addressed:** ramy.aboushelbaya@physics.ox.ac.uk

ABSTRACT

In this article, we showcase the experimental results of methods to produce and characterize orbital angular momentum (OAM) carrying high-power lasers. The OAM pulses were produced on the ASTRA laser of the Central Laser Facility using a continuous spiral phase plate. Three different characterization methods were then used to measure the OAM content of the beam. The methods that were used were a cylindrical lens diagnostic, an interferometric diagnostic, and a projective diagnostic. We further discuss the relative advantages and disadvantages of each method in the context of high-power laser experiments.

I. INTRODUCTION

High-power laser pulses have been an important part of scientific research ever since the invention of chirped-pulse amplification (CPA) made their generation a more feasible task. They are essential for a diverse set of fields ranging from applied research into laser-plasma physics such as laser wakefield acceleration[1] to more fundamental investigations into laser–plasma interactions and probing non-linear vacuum quantum electrodynamic (QED) effects.[2] As such, a large amount of research has been made into the characterization of the temporal and spatial profiles of these high-power pulses.

The orbital angular momentum (OAM) of light is a quantized degree of freedom of electromagnetic radiation that is characterized by an azimuthal phase dependence in the transverse profile of the beam $u(\rho, \phi) \propto e^{il\theta}$, where $u(\rho, \phi, z)$ is the function, which characterizes the transverse profile in cylindrical coordinates, and l is the azimuthal mode number, which quantizes the OAM of the mode. Unlike the more familiar spin angular momentum (SAM), which is related to the circular polarization states of light, OAM is unbounded and can take any integer value. Ever since Allen *et al.* first characterized the OAM of the Laguerre–Gaussian (LG) solutions to the electromagnetic wave equation,[3] the interest in OAM has steadily grown. Since it is unbounded and can have any integer value, OAM has seen many applications in different fields including enhanced imaging techniques,[4] light manipulation, and high density coding of information for communication.[5] Consequentially, over the course of the previous two decades, the techniques required to efficiently generate OAM states and detect and filter photons according to their OAM state (right down to the single-photon level[6]) have been honed to a great level of precision. Due to most of the research having been concentrated in classical and quantum optics, these techniques mostly focused on low-powered tabletop lasers and even single-photon sources.

However, the interest in OAM did not remain confined in the aforementioned fields. Over the past decade, there has been growing research interest in exploring its effects on laser–plasma interactions, in particular when it comes to parametric instabilities such as the Raman and Brillouin instabilities.[7] This is in addition to research in exploiting the various properties of OAM to enhance laser-wakefield acceleration[8] and to provide an additional signature for laser-QED effects.[9] In order for experimental research to be successfully accomplished to evidence any of these theoretical findings, methods to

reliably and efficiently generate and measure the OAM of high-power lasers must be developed.

To that end, we have conducted an experimental campaign on the ASTRA laser of the Central Laser Facility (CLF) in order to test the applicability of three different methods for characterizing orbital angular momentum in the context of high-power laser pulses and investigate their relative strengths and weaknesses. These three methods are based on methods to characterize low-power CW lasers and single photon sources. In this paper, we report the results of the experiments. This paper will be organized as follows: first, a short recap of the basic theory of the OAM of electromagnetic modes will be presented. Following this, the method for generating high-power OAM-carrying pulses, as well as the specifications of the ASTRA laser, will be outlined. Then, three different characterization methods will be explored, and the experimental results of their performance will be showcased. This will be followed by a discussion of the advantages of each method and its suitability for specific applications. Finally, we will conclude with an overview of the future planned work.

II. THE ORBITAL ANGULAR MOMENTUM OF LIGHT

Considering the propagation of light in the vacuum, an electromagnetic wave can be fully described by its electric field vector $\mathbf{E}(\mathbf{r}, t)$ (the magnetic field can be derived from Maxwell's equations), which obeys the electromagnetic wave equation,

$$\frac{1}{c^2}\frac{\partial^2 \mathbf{E}}{\partial t^2} - \nabla^2 \mathbf{E} = 0. \tag{1}$$

It is well known that the energy flux of an electromagnetic wave is represented by its Poynting vector defined via the physical fields as

$$S = \frac{1}{\mu_0}(\mathbf{E} \times \mathbf{B}), \tag{2}$$

from which we can then define the linear momentum density of the wave,

$$p = \frac{\langle S \rangle}{c}, \tag{3}$$

which can be integrated to form the total linear momentum carried by the wave $P = \iiint p dV$. Analogously, we can define the total angular momentum carried by the wave as

$$J = \iiint j dV = \iiint \mathbf{r} \times (\mathbf{E} \times \mathbf{B}) dV. \tag{4}$$

It can be shown that when considering propagation media other than the vacuum, where an electromagnetic wave may interact with charged particles, Eq. (4) represents the contribution of the wave to the conserved total angular momentum of the system, thus confirming its interpretation as the angular momentum of light. Considering the solutions to the paraxial wave equation in cylindrical coordinates, these can be expanded onto a basis of the so-called "Laguerre–Gaussian" modes,

$$\mathbf{E}_p^l(\mathbf{r}) = \sqrt{\frac{2p!}{\pi(|l|+p)!}}\frac{w_0}{w(z)}\left(\frac{\rho\sqrt{2}}{w(z)}\right)^{|l|}\exp\left(-\frac{\rho^2}{w^2(z)}\right) \tag{5}$$

$$\times L_p^{|l|}\left(\frac{2\rho^2}{w^2(z)}\right)\exp\left(-i\left(\frac{k\rho^2}{2R(z)} + l\phi - \psi(z)\right)\right)\hat{\mathbf{e}}_\sigma, \tag{6}$$

where $w(z)$, $R(z)$, and $\psi(z)$ are the typical beam width, radius of curvature, and Gouy phase shift of Gaussian modes; w_0, l, and p are the beam waist at focus, azimuthal mode number, and radial mode number, respectively; and $L_p^l(x)$ is the generalized Laguerre polynomial. $\hat{\mathbf{e}}_\sigma = \hat{\mathbf{x}} + i\sigma\hat{\mathbf{y}}$ is the polarization vector, where $\sigma \in \{\pm 1, 0\}$, indicating right, left-circular, or linear polarization. Putting these solutions in the definition of the total angular momentum, we can show that for LG modes, $J \propto (l + \sigma)$, where one component arises from the polarization of the field and the other from the azimuthal dependence of the spatial structure.[3]

Figure 1 showcases different transverse profiles of the electric fields of different LG modes. In the case of modes where $p = 0$ and $l \in \mathbb{Z}^*$ [such as the ones shown in Figs. 1(b) and 1(c)], if we would plot the intensity of the beam averaged over one wavelength, we would get the distinctive "doughnut" shape of OAM modes. The question then arises how best to generate high-powered laser pulses carrying OAM. From this point, we will restrict our discussion to modes where the radial mode number is null.

III. GENERATING OAM-CARRYING HIGH-POWER PULSES

One of the earliest ways to generate beams carrying OAM was to use forked phase holograms.[10] Like other types of holograms,[11] they encode information concerning the interference between the phase of a regular Gaussian wavefront and a LG one, which cross at a particular angle. When a normal Gaussian pulse is then shown on this forked hologram, different orders of diffraction produce higher order OAM modes. These holograms can even be blazed so as to maximize the amount of energy that is put into the desired OAM mode.[12] As such, they have proven to be quite effective at OAM conversion for low-powered continuous and pulsed sources across a range of applications. They, however, become highly impractical when attempting to use

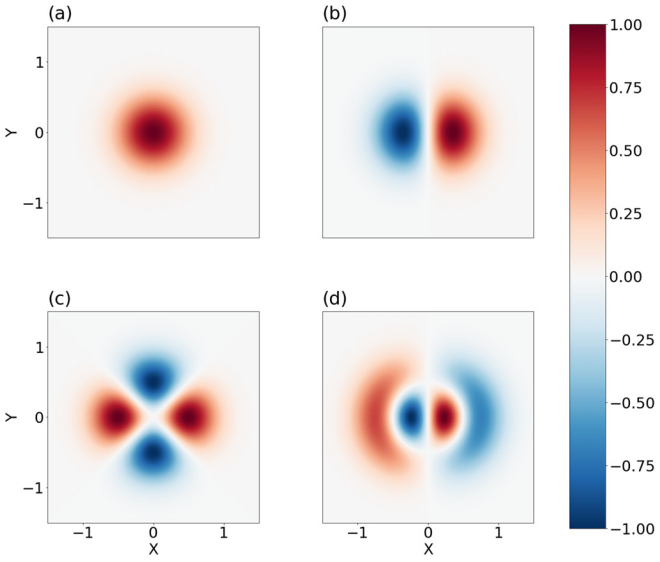

FIG. 1. Different transverse profiles for the simulated electric fields of various Laguerre–Gaussian modes with (l, p) = (a) (0, 0), (b) (1, 0), (c) (2, 0), and (d) (1, 1). The amplitude of these modes has been normalized so that their maximum would be 1.

them on a full high-powered pulse. Unlike the mW-scale lasers used in low-power applications, which can have beam diameters smaller than 1 cm, high-power lasers need to be expanded in order to minimize their intensity and fluence protecting the optical components from any damage. This means that these holograms, which generally have highly detailed micrometer-scale features especially around the "fork," need to be quite large in order to fit the whole beam, making their fabrication a significant technical challenge. Recently, it has been shown that using two relatively "weak" pulses, one can generate a holographic pattern in a plasma, which can then be used to impart OAM on an ultra-intense pulse, which diffracts off it in a manner similar to phase holograms made from dielectric media.[13] However, these plasma holograms require very precise spatiotemporal alignments of the driving short pulses and precise alignment of the input pulse that needs to be converted.

A relatively simpler alternative is to turn to what are called spiral phase plates (SPPs). These are plates that impart an azimuthally varying phase on the wavefront of any incoming beam. Consider, for example, the model, shown in Fig. 2, of a typical continuous transmissive SPP; when a beam with a planar phasefront passes through the SPP, it acquires different relative phase shifts based on the azimuthal angle due to the varying thickness of the plate since we want the beam to acquire a relative phase factor $\propto e^{il\phi}$ after passing through the SPP. The thickness of the plate as a function of the azimuthal angle can be mathematically modeled as

$$h(\phi) = \frac{l\lambda\phi}{2\pi\Delta n} + h_0, \tag{7}$$

where λ is the wavelength of the light in question, l is the desired OAM state, $\Delta n = n_{\mathrm{SPP}} - n_{\mathrm{air}}$, and h_0 is the thickness of the base of the SPP before the helical part. In particular, the height of the step discontinuity of the plate is $h = l\lambda/\Delta n$. For our tests, we have built a continuous SPP made of polymethyl methacrylate (PMMA) with a diameter of 100 mm. A diameter of this size is required in order to accommodate the aforementioned large beam diameters of high-power lasers. This plate was designed for the ASTRA laser at the Central Laser Facility (CLF). The ASTRA beam is an 800 nm laser, which delivers up to 600 mJ of energy in 50 fs. The beam diameter at the exit of the compressor comes to 60 mm. Figure 3 shows the focal spot of the ASTRA laser after it had went through the SPP where the beam was apertured to 20 mm in order to be able to see the distinctive "doughnut" shot typical of an OAM beam.

FIG. 2. 3D model of a spiral phase plate showing the discontinuity in the azimuthally varying thickness. The height of the step controls the amount of OAM a specific wavelength of light will acquire.

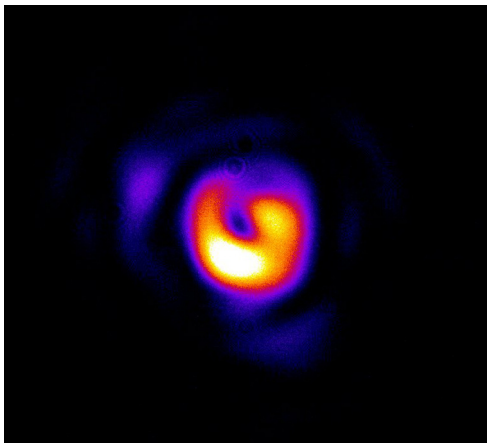

FIG. 3. The focal spot of the ASTRA laser after passing through the transmissive continuous spiral phase plate. The beam has been apertured from its full size down to 20 mm to increase the size of the focal spot in order to better resolve the spatial structure imparted by the SPP and to avoid the step height inhomogeneity that existed on the plate away from its center. As can be clearly seen from the image, the spot shows the distinctive singularity near the center due to the phase discontinuity caused by the azimuthal dependence.

In order to fabricate the plate, we turn it out of a stock material. The rear surface of the plate is skimmed to ensure that it is parallel to the machine axis and is flat with no waviness as any variation would cause the step in the SPP to be lost. We then skim the active face flat as well with respect to that zero plane. The machine then runs the cutting program to shave the form into the surface. The plate is not held with a vacuum chuck as that would distort the surfaces when machining. The spacing of the cuts, tool speed, start diameter, and helix depth are all optimized to ensure the best cutting performance, and the depth of the step is limited by the swarf pick on the tool. It is measured using a white light interferometer to determine the step height of the SPP across its radius, and this is then fed back to optimize the programming.

There are various difficulties and challenges that arise when using transmissive spiral phase plates to generate OAM-carrying beams. First, for the plate to work as expected, the incoming beam must have a relatively flat phase front in order to produce the best quality OAM beams at the output. This generally can be arranged as most high-power laser facilities have a way to correct any wavefront aberrations using adaptive optics and wavefront sensors. The same tools can then be used to optimize the beam produced by the SPP. Additionally, there are mechanical concerns when it comes to fabricating these plates. Since they are transmissive, we would like to have them as thin as possible in order to minimize any B-integral or non-linear effects driven by the high-powered lasers that will be propagating through them. Although the thickness of the step is quite small (on the order of the wavelength of the light it is designed for), the base of the plate needs to be thick enough to prevent any warping effects and to keep it stable and flat. This becomes even more crucial as the size of the plate increases to accommodate larger laser diameters. This thinness/stability trade-off effectively puts a power-threshold on the usability of these transmissive plates.

For our particular plate specifically, there were particularly many difficulties in maintaining a consistent height along an entire radial

line due to the continuous nature of the plate and its large diameter. This inhomogeneity made the plate incapable of adequate conversion for the full-sized 60 mm ASTRA beam. As such, in order to perform our diagnostic tests, we were forced to only use it with the beam apertured to 20 mm as the height of the SPP was fairly consistent over that length.

A more promising method of OAM conversion can be found in reflective spiral plates. They are similar in principle to the transmissive ones in the sense that they operate by imparting an azimuthally varying phase factor onto an incoming beam. As the name suggests, however, this is done by having a reflective surface that has an azimuthally varying height from a specific base. As such, they circumvent any issues associated with the transmission of high-power beams through dielectric media. That way, they can be as thick as needed to make them stable, and they can be made from materials that withstand even the most powerful lasers in operation. They can even be fabricated in such a way so as to operate off-axis,[14] reflecting the beam at an angle and avoiding any geometrical issues with their inclusion in experimental setups.

IV. CHARACTERIZING ORBITAL ANGULAR MOMENTUM

The fact that OAM-carrying beams have a very distinctive transverse spatial structure with the singularity present at the center of the intensity profile alone does not suffice to characterize these modes. The singularity could potentially be due to other effects, and even if it is simply due to the presence of OAM, it would not be possible to accurately gauge the amount of OAM present nor its orientation. As such, more sophisticated methods are required in order to be able to analyze the results of experiments involving the interaction of high-power OAM-carrying modes. Of course, the most comprehensive method would be to use a wavefront sensor to measure the phase information contained within the beam profile. However, this is highly impractical as most wavefront sensors lack the resolution required to completely acquire all the phase information over the relatively large diameter of these beams. Additionally, these sensors are highly sensitive to alignment and any other aberrations that are bound to exist in physical situations.

As mentioned above in Sec. I, much of the research into characterizing the OAM of light has been focused on low-power beams and even single-photons. This is due to the fact that the vast majority of experiments involving OAM have been in that regime, while the application of OAM to high-power interactions has mostly remained in theoretical and numerical research so far. For a characterization method to be suited for use in high-power laser applications, it must meet some important criteria: first, it needs to be able to measure collective electromagnetic effects (not single-photons). Depending on the type of high-power facility, additional constraints must be met. For low-energy high-intensity facilities, it also needs to be able to measure short to ultra-short pulses (ps down to fs-scale). For high-energy facilities with ns, it needs to be able to perform the measurement in a single-shot since the repetition rate on high-power laser facilities can be quite low, and there are often issues with shot-to-shot reproducibility. This section will showcase the results of an experimental investigation into the practicality of three different methods for characterizing OAM as they apply to high-power pulses.

A. Cylindrical lens diagnostic

It is well known that lenses, arranged in particular configurations, can be used to immediately compute the spatial Fourier transform of the transverse spatial profile of the input light field. In particular, a one-lens imaging system would produce, at the focal plane, a field whose magnitude is equivalent to the magnitude of the spatial Fourier transform of the input field. However, as seen in Sec. III, the information contained in the focal plane of a spherical lens would not be sufficient to characterize the OAM on the input field. However, it has been shown that cylindrical lenses, which only focus along one particular spatial axis leaving the other intact, produce very distinctive shapes at their focal planes when a collimated OAM-carrying mode is incoming on them.[15]

In fact, the intensity $I(x_f, y_f)$ at the focal plane (x_f, y_f) of a simple one-cylindrical lens optical system can be modeled as the magnitude of a one-dimensional Fourier transform of the two-dimensional function describing the transverse profile of the input LG mode $E_p^l(x_i, y_i)$ at the input plane (x_i, y_i),

$$I_p^l(x_f, y_f) \propto \left| \int E_p^l(x_i, y_f) e^{i2\pi x_f x_i/\lambda f}\, dx_i \right|^2, \tag{8}$$

where λ is the wavelength of the incoming light and f is the focal length of the cylindrical lens. There are two subtleties here, which should be noted. This form assumes that the cylindrical lens has been perfectly aligned so as to act along some well-defined spatial x-axis. However, the choice of the x-axis is of course completely arbitrary and, in the case of LG modes, irrelevant since rotations in the transverse plane would only amount to adding a constant phase factor, which is physically meaningless. In experimental conditions, the rotation of the cylindrical lens around the axis of propagation of the incoming beam would be adjusted for the convenience of the setup and subsequent data analysis but would not impact the information contained within. The second point is that although the cylindrical lens only acts along the x-axis, technically, there are diffraction effects on the y-axis from the plane of the lens y_i to the focal plane y_f. However, since we are considering a collimated input beam with a Rayleigh length that is larger than any of the relevant physical dimensions of the system, these effects can be ignored.

Figures 4(a)–4(d) show simulated results of the action of a cylindrical lens on various LG modes $E_l^0(x_i, y_i)$. These simulations clearly show that for LG modes with $l \neq 0$, there are fringes that appear. The number of dark fringes corresponds to the absolute value of different l mode numbers. Not only that, the tilt of the fringes changes with the sign of l. This means that in one shot, this diagnostic is capable of providing information concerning both the magnitude and the orientation of the OAM carried by the mode. It is important to note that there is no "absolute" sign for the OAM of light, and it is only meaningful to speak of the relative sign of one with respect to another. In fact, Eq. (8) can be solved for particular values of l so that the experimental data may be compared to the ideal solution. For example, solving the equation for the first LG modes with unit waist gives

$$I_{\pm 1}^0(x_f, y_f) \propto \exp\left[-\left(\frac{k^2}{4} + y^2\right)\right](k \pm 2y), \tag{9}$$

$$I_{\pm 2}^0(x_f, y_f) \propto \exp\left[-\left(\frac{k^2}{4} + y^2\right)\right](-2 + (k \pm 2y)^2). \tag{10}$$

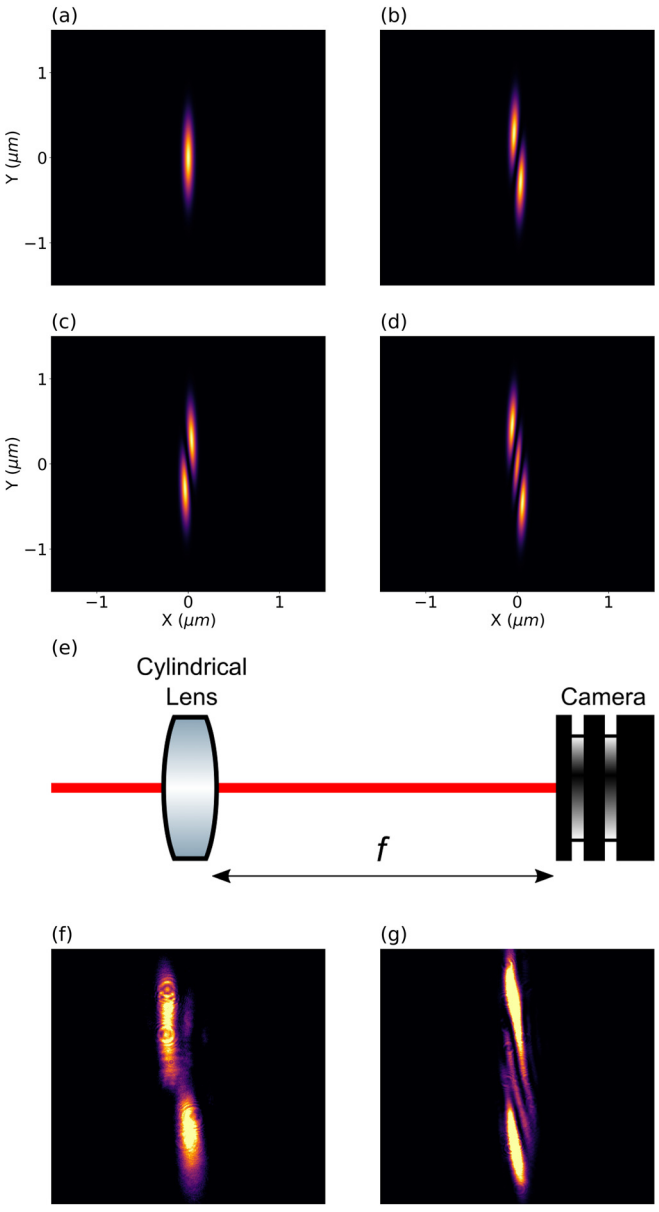

FIG. 4. (a)–(d) Simulated norm of a one-dimensional Fourier transform performed along the transverse *x*-axis of different Laguerre–Gaussian modes with $l = 0, +1, -1, +2$, respectively. The simulated norms clearly show the distinctive fringe pattern caused by the OAM. (e) Optical setup for the diagnostic that was built at the ASTRA target area. (f) Experimental result from a shot of the ASTRA laser after going through the SPP clearly showing the pattern similar to the $l = 1$ simulated pattern shown above. (g) Experimental result from a continuous low-power 400 nm beam after it went through the same SPP placed in the opposite orientation.

Figures 4(f) and 4(g) show some experimental results using this diagnostic on both an ASTRA main beam shot and a much weaker mW CW laser diode emitting light at $2\omega_{\mathrm{ASTRA}}$ after they had gone through the SPP. The output of the diagnostic fits well with what is to be expected from these beams. For the laser diode, the SPP was put in the opposite direction to showcase the ability of this diagnostic to distinguish the sign of the OAM, which is clear from the image seen at the focal plane. Additionally, the laser diode emits at twice the frequency of the ASTRA beam, which means that it will acquire twice the azimuthal charge going through the SPP and subsequently twice the OAM. For this reason, the result of the diagnostic shows two dark fringes characteristic of $l = 2$.

This diagnostic has many important advantages that make it well suited for use in high-power laser systems. It is based on a single optical component and a single sensor component as it requires very little alignment. Additionally, reflective cylindrical optics are available, which would allow for the characterization of even more high-powered beams where the intensity would damage traditional transmissive cylindrical lenses. It also gives us information both on the magnitude and the orientation of the OAM in one easy-to-interpret output. Space-wise, since it requires so few components, this diagnostic can be made arbitrarily compact by using a cylindrical optic of appropriate focal length. It should be noted, however, that if the F-number (f/D, with f being the focal length and D the diameter of the beam) of the system is too small, this will result in a very small spatial extent in the direction of the focusing. This might make interpreting the output difficult, or even impossible, depending on the spatial resolution of the sensor being used. However, this problem can be circumvented by aperturing the input beam reducing the F-number of the system. A shortcoming that cannot be avoided, unfortunately, is that if the input beam to the diagnostic is composed of a superposition of various OAM modes, then it will be relatively difficult to accurately decompose them since the only data that would be in the output are the magnitude of the sum of their various Fourier transforms.

B. Interferometric OAM diagnostic

Another common way of characterizing structured spatial phase variations is by interfering the beam with another reference one that carries a well-defined OAM (such as a Gaussian $l = 0$ beam). This allows for extracting certain information about the phase of the original beam. However, this is impractical when it comes to high-power laser experiments as that requires precise alignment (in space and time) of the pulse with another reference pulse that is similar enough in amplitude and wavelength. A way around these restrictive conditions is to interfere the pulse with a copy of itself. However, for this to give any useful information on the azimuthal charge, there must be a way to modify the transverse profile of one copy relative to another. This can be done using optical components known as prisms.[16] In our case, we used what is called a dove prism. A dove prism is a transparent hexahedron where the four lateral sides are regular trapezoids, and the top and base are different sized rectangles. It can be used to rotate the transverse profile of an input beam or to create a mirror image of it. In our case, we are interested in its ability to rotate an input OAM beam, which, as mentioned previously, amounts to adding a relative phase shift.

Our setup is based on the well-known Mach–Zehnder (M–Z) interferometer. As shown in Fig. 5(a), two dove prisms are introduced into each of the M–Z interferometer's arms. The prisms are rotated by $\alpha = \pi/2$ with respect to each other. This causes one copy of the input beam to be rotated by $2\alpha = \pi$ relative to the other. In the case of an LG mode, this would mean that the transverse spatial variation of the

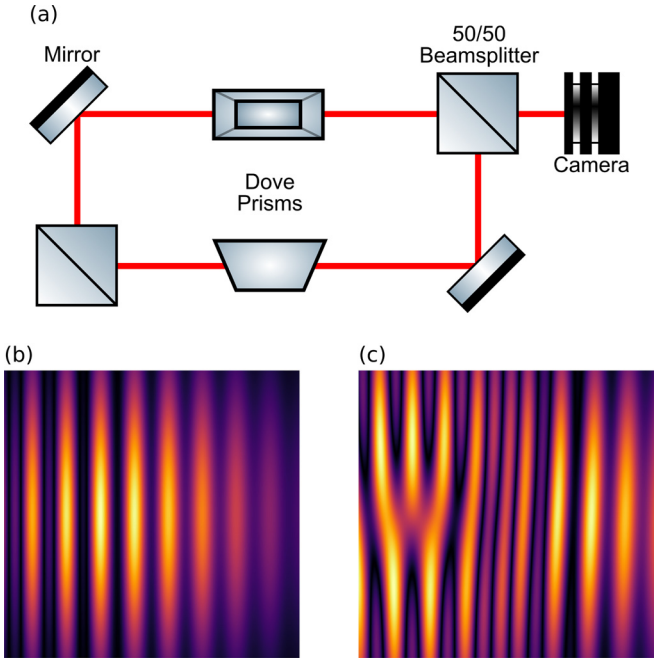

FIG. 5. (a) Basic schematic showing the optical setup for the OAM interferometer. (b) and (c) Simulated results for the output of the interferometer in the case of a normal Gaussian profile and a LG with $l = 1$, respectively.

phase of one copy will be 180° out of phase with the other. This signifies that when the M–Z inteferometer is perfectly aligned, even OAM modes would favor one path after the final beam splitter, while odd modes would favor another. This can be used to create an "OAM-splitter" for single photons.[6]

However, this splitting is not very relevant for our purposes as we are currently interested in characterizing macroscopic fields and not single photons. Another consequence of this setup can be seen when the interferometer is not perfectly aligned so as to create interference fringes at the outputs of the final beam splitter. As can be seen in Figs. 5(b) and 5(c), the interference between a beam and a rotated copy of itself creates distinctive patterns depending on the l mode number. For a regular Gaussian $l = 0$, the pattern is the standard fringes normally seen in such interferometers. For $l = 1$, the fringes present with a distinctive "fork" shaped discontinuity similar to the one present in the aforementioned phase holograms. These varying patterns make it possible to diagnose different OAM states of the beam. Again, they hold information not only on the magnitude of the beam but also on its relative orientation. For example, the pattern for $l = -1$ would be inverted relative to the one for $l = 1$.

The setup shown in Fig. 5(a) was built and aligned at the CLF and tested on the ASTRA laser. Due to the relative complexity of the setup, it was done on multiple stages. First, a standard Mach–Zehnder interferometer was built and aligned using a continuous source to first align the direction of the two copies in order to see the standard interference fringes on one of the two outputs of the final beam splitter. Although the arms of the interferometer were adjusted so as to have two approximately equal path lengths, some final alignment is always needed using a delay stage on which one of the mirrors is fixed. This allows us to fine-tune the path length to optimize the interference when switching to pulsed beams. This becomes especially crucial when dealing with fs pulses such as the ASTRA laser. Once the alignment and optimization of the Mach–Zehnder are complete, dove prisms with the desired relative rotations are inserted into each path. The orientation and position of the dove prisms are then adjusted to first retrieve the interference fringes with the continuous beam. Although the dove prisms are chosen to be of the same size, uncertainties in the manufacturing can be large enough to cause temporal misalignment for fs pulses. This can be compensated for by using the aforementioned delay stage. As can be seen from the results shown in Fig. 6, the behavior of the beam is similar to the one shown in the previously discussed simulated results. The interferometric diagnostic allows us to distinguish between a regular Gaussian beam and a $l = 1$ beam.

Although this diagnostic offers a way to quantify the OAM state (both magnitude and relative orientation) of a pulsed beam, it suffers from many shortcomings. The setup is complex, the alignment is quite involved and time-consuming, and any slight drift in the direction of propagation of the input pulse might cause the diagnostic to fail. This only gets exacerbated as the pulse length decreases because the system then becomes even more sensitive to temporal misalignment and hence the need for the delay stage in the Mach–Zehnder interferometer. For example, the ASTRA pulse, at 50 fs, would get temporally misaligned if the two paths in the interferometer were to drift by 15 μm. Since many high-power lasers tend to use even shorter pulses, this makes this drawback particularly critical. Besides the practical implementation aspects of this diagnostic, it has other more fundamental disadvantages. Although it is relatively easy to diagnose the $l = 0, \pm 1$ OAM states from the pattern in the output image, this is not at all the case for higher order modes. Figure 7 showcases the complex interference patterns that emerge from pure high-order OAM states. In fact, high-order modes would generate patterns that would require ever increasing spatial windows to properly diagnose. Additionally, in an actual experiment, the modes being diagnosed are rarely pure OAM modes. As such, the emerging patterns would be even more difficult to diagnose and fit to simulated data.

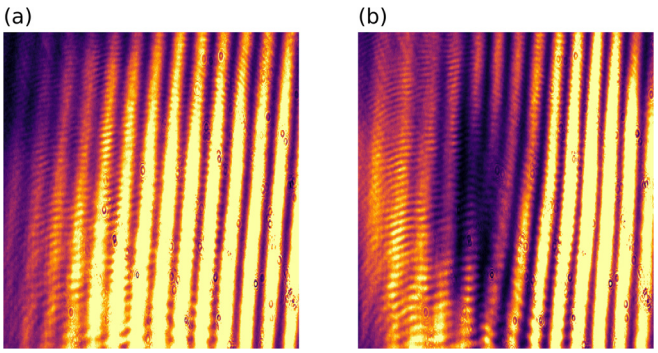

FIG. 6. Experimental results for the interferometric diagnostic on the ASTRA laser. (a) The result for the standard beam without the SPP, so $l = 0$, shows the typical fringes usually seen in interferometers. (b) When the SPP is placed in the beam path, the profile of the fringes changes and a discontinuity similar to the one in Fig. 5(c) is seen, indicating the presence of OAM.

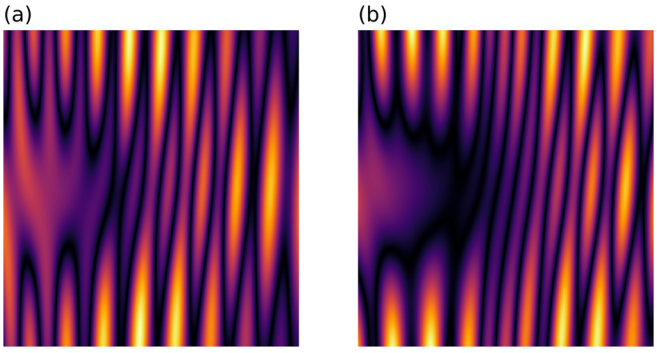

FIG. 7. Simulated results of the output of the interferometric diagnostic for (a) $l = 2$ and (b) $l = 3$. As can be seen from (a) as compared to Fig. 5, the LG_0^2 mode has a fork shape but with two inner prongs instead of one. For LG_0^3, the pattern becomes extremely difficult to identify and exceeds the size of the window.

C. OAM projective measurement

So far, the diagnostic methods that have been discussed have shown some weaknesses when faced with non-pure OAM states. The last one that will be discussed offers a way around this problem. This is done by "projecting" the input beam onto various OAM basis states. The basic principle around this projective method is the fact that any beam can be filtered from its non-Gaussian components through using a spatial mode filter, such as a pinhole. Consider a setup such as the one in Fig. 8; if one would split the input beam with l_{in} into multiple paths and put a known OAM mode converter on each path [such the aforementioned phase holograms or spatial light modulators (SLMs)], then each beam on each path j would have an OAM state of $l_{in} + l_j$. This means that on each path j, the component of the beam, which has the OAM of $-l_j$, will be converted into a Gaussian mode, while other components will convert to various other modes. This means that if the beam were to be focused on a spatial mode filter placed after the mode converter followed by a detector, only the $-l_j$ component will be passed through the filter and be detected. An additional path can be added, which has no filters or mode converters; this allows for the detection of the power that is in the rest of modes not being projected by the other paths.

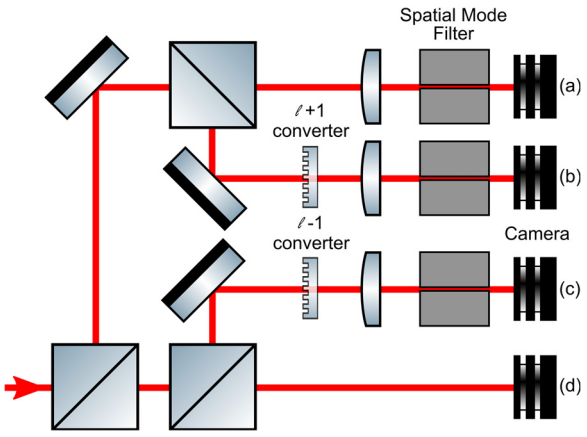

FIG. 8. Schematic of an example of a projective diagnostic capable of projecting on $l = 0$ along path (a), $l = -1$ along path (b), and $l = 1$ along path (c). The remainder components of the beam can be inferred from the control measurement along path (d).

To test the operation of this diagnostic method, we opted to project on just one state in order to calculate the Gaussian component that is left in the beam after the OAM conversion. This was done because fabricating spatial mode converters for beams of the size typically used in high-power laser experiments is quite a complex and difficult process. The spatial mode filter that was used was a single mode step-index optical fiber cable optimized for use for 800 nm light. When an external beam is coupled into a fiber-optical cable, it has the potential to excite a variety of waveguide modes. For the vast majority of use cases, the waveguide modes of interest are the so-called weakly coupled linearly polarized modes LP_m^l,[17] where l and m serve a similar purpose as in the free-space LG_m^l modes. The single mode step-index fiber is one where the V number is less than 2.4 for its wavelength of operation λ, where V is defined as

$$V = \frac{2\pi a}{\lambda}\sqrt{n_1^2 - n_2^2}, \tag{11}$$

with a being the diameter of the core, n_1 the refractive index of the core, and n_2 the refractive index of the cladding. When the aforementioned condition is satisfied, only the fundamental LP_1^0 (analogous to the free-space Gaussian) is guided in the fiber. In such a cable, any higher-order mode, which gets excited, decays quickly in an exponential manner $I \propto e^{-\alpha L}$, where α is the attenuation coefficient and L is the length of the cable. It should be noted that a fiber optic cable is only single-mode above a particular wavelength, termed the "cutoff" wavelength. Below this threshold, high-order modes can be guided. In practical use, the cut-off wavelength is generally defined as that where the attenuation of the second mode LP_1^1 is 20 dBm^{-1} more than the fundamental mode.[18] The higher the wavelength relative to the cutoff, the more the high-order modes are attenuated. Experiments have shown that the attenuation can be as high as 25 dBm^{-1} for single photons.[19] In our setup, we used a one-meter long single-mode optical fiber where the cutoff was at 730 nm, well below the wavelength of the Astra beam. Detecting the power of the beam after the filter, and adjusting for the action of the filter and the transmission of the SPP, shows that 27% of the power remains in the Gaussian beam. This signifies that the transmissive SPP has a conversion efficiency of around 73% into non-Gaussian modes.

Since this characterization method is capable of identifying and quantifying an arbitrary number of LG_0^l components present in a beam with very little post-processing, it is technically the most complete way to characterize the OAM of any beam. However, it does have several important drawbacks that limit its practicality. First, the alignment procedure can be very involved depending on the number of modes one wishes to project on. Each additional path requires at least four components aligned: a mode converter, a lens, a mode filter, and a camera/photodetector. This makes the device poorly scalable. This is also aggravated by the fact that any misalignment in one particular path relative to the others would make it more difficult to interpret the results of the diagnostic. Additionally, mode converters can be quite difficult to make, especially if they need to accommodate the beam size and intensity of high-power laser pulses. This brings us to the final, and perhaps most salient, limitation of the device when it comes to its use with high-power beams. Although there are fiber

TABLE I. Summary of the main differences between the three diagnostic methods that were considered to show their relative strengths and weaknesses. The scalability is measured as a function of the number of OAM modes n one wishes to detect.

Diagnostic	Difficulty of alignment	Post-processing required	Mixed modes	Scalability
Cylindrical lens	Easiest	Moderate	No separation	$O(1)$
Dove prism interferometer	Moderate	Considerable	No separation	$O(1)$
Projective measurement	Difficult	Minimal	Completely separated	$O(n)$

cables designed for high-power use, almost all high-power beams would require heavy attenuation if fiber cables are to be used to directly diagnose their OAM. An alternative, and more suitable, solution would be to use pinhole filters, which can made be from materials that can easily withstand much higher intensities. There have even been pinhole filters capable of withstanding up to[20] 3×10^{12} W/cm^2.

V. CONCLUSION

In this paper, we explore the relative advantages and disadvantages of three different orbital angular momentum diagnostics in the context of high-power laser experiments. We also discuss results from an experimental campaign on the Astra laser designed to field test each of these diagnostics and a method for generating OAM carrying beams using continuous transmissive spiral phase plates (SPPs). As can be seen in Table I, the cylindrical lens diagnostic and the projective measurement offer significant advantages, each in particular use cases. The cylindrical lens diagnostic is the least resource-intensive and the easiest diagnostic to align. Since its action on the input beam can be easily modeled mathematically, it still produces a relatively simple to process output. On the other hand, the projective measurement method gives us the most complete diagnostic of the OAM content of the beam in terms of the integer-indexed OAM basis modes. However, this comes at a cost of the increased complexity of its setup. By contrast, the interferometric method sits well in the middle and offers no advantages that can be had by the other two methods.

The main goal of the experiment whose results were detailed in this paper was to identify the pitfalls and best practices for using high-intensity pulses carrying OAM. This has led to a currently planned experiment to evidence photon–photon scattering in vacuum using real photons. Although many setups have been proposed to witness this effect such as in Ref. 2, using high-power pulses, they suffer from a low signal-to-noise ratio (SNR). Recently, it has been shown[9] that OAM can provide a unique identifying signature to evidence to improve the SNR by over 20 dB. Figure 9 showcases the proposed experimental setup, which uses the projective diagnostic method explained in Sec. IV to filter unwanted OAM modes arising from various experimental noises.

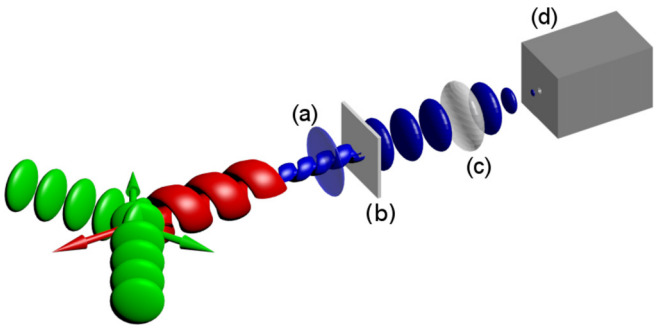

FIG. 9. Planned schematic for the photon–photon scattering detection experiment. (a) Narrow-band wavelength filters eliminate light at undesirable frequencies. (b) Mode converters only convert the appropriate OAM mode to Gaussian. (c) Lens to focus the radiation on the spatial mode filter. (d) Spatial mode filter leading to a photodetector.

ACKNOWLEDGMENTS

The authors would like to thank the staff of the Central Laser Facility (CLF), and in particular, Dr. Yiftach Katzir, for their invaluable help and support, which led to the results presented in this work. This work was supported by UKRI-STFC and UKRI-EPSRC under Grant Nos. ST/P002048/1 and EP/N509711/1. R.A. acknowledges support from the St Anne's Graduate Development Scholarship scheme. We also gratefully acknowledge support from the Oxford-ShanghaiTech collaboration project and UKRI-STFC under Grant No. ST/T000724/1. This project received funding from the European Union's Horizon 2020 research and innovation programme under Marie Skłodowska-Curie Grant Agreement No. 665593 awarded to the Science and Technology Facilities Council.

DATA AVAILABILITY

The data that support the findings of this study are available from the corresponding author upon reasonable request.

REFERENCES

[1]S. M. Hooker, "Developments in laser-driven plasma accelerators," Nat. Photonics **7**, 775–782 (2013).
[2]E. Lundstrom, G. Brodin, J. Lundin, M. Marklund, R. Bingham, J. Collier, J. T. Mendonça, and P. Norreys, "Using high-power lasers for detection of elastic photon-photon scattering," Phys. Rev. Lett. **96**, 083602 (2006).
[3]L. Allen, M. W. Beijersbergen, R. J. C. Spreeuw, and J. P. Woerdman, "Orbital angular momentum of light and the transformation of Laguerre-Gaussian laser modes," Phys. Rev. A **45**, 8185–8189 (1992).
[4]R. Gozali, T.-A. Nguyen, E. Bendau, and R. R. Alfano, "Compact OAM microscope for edge enhancement of biomedical and object samples," Rev. Sci. Instrum. **88**, 093701 (2017).
[5]Y. Ren, Z. Wang, G. Xie, L. Li, Y. Cao, C. Liu, P. Liao, Y. Yan, N. Ahmed, Z. Zhao, A. Willner, N. Ashrafi, S. Ashrafi, R. D. Linquist, R. Bock, M. Tur, A. F. Molisch, and A. E. Willner, "Free-space optical communications using orbital-angular-momentum multiplexing combined with MIMO-based spatial multiplexing," Opt. Lett. **40**, 4210–4213 (2015).
[6]J. Leach, M. J. Padgett, S. M. Barnett, S. Franke-Arnold, and J. Courtial, "Measuring the orbital angular momentum of a single photon," Phys. Rev. Lett. **88**, 257901 (2002).

[7]J. T. Mendonca, B. Thidé, and H. Then, "Stimulated Raman and Brillouin backscattering of collimated beams carrying orbital angular momentum," Phys. Rev. Lett. **102**, 185005 (2009).
[8]J. Vieira, J. Mendonça, and F. Quéré, "Optical control of the topology of laser-plasma accelerators," Phys. Rev. Lett. **121**, 054801 (2018).
[9]R. Aboushelbaya, K. Glize, A. Savin, M. Mayr, B. Spiers, R. Wang, J. Collier, M. Marklund, R. Trines, R. Bingham, and P. Norreys, "Orbital angular momentum coupling in elastic photon-photon scattering," Phys. Rev. Lett. **123**, 113604 (2019).
[10]J. Arlt, K. Dholakia, L. Allen, and M. J. Padgett, "The production of multiringed Laguerre-Gaussian modes by computer-generated holograms," J. Mod. Opt. **45**, 1231–1237 (1998).
[11]W. T. Cathey, "Phase holograms, phase-only holograms, and kinoforms," Appl. Opt. **9**, 1478–1479 (1970).
[12]A. Nicolas, L. Veissier, L. Giner, E. Giacobino, D. Maxein, and J. Laurat, "A quantum memory for orbital angular momentum photonic qubits," Nat. Photonics **8**, 234–238 (2014).
[13]A. Leblanc, A. Denoeud, L. Chopineau, G. Mennerat, P. Martin, and F. Quéré, "Plasma holograms for ultrahigh-intensity optics," Nat. Phys. **13**, 440–443 (2017).
[14]A. Longman, C. Salgado, G. Zeraouli, J. I. Apinaniz, J. A. Perez-Hernandez, M. K. Eltahlawy, L. Volpe, and R. Fedosejevs, "Off-axis spiral phase mirrors for generating high intensity optical vortices," arXiv:2001.07813 (2020).
[15]S. N. Alperin, R. D. Niederriter, J. T. Gopinath, and M. E. Siemens, "Quantitative measurement of the orbital angular momentum of light with a single, stationary lens," Opt. Lett. **41**, 5019–5022 (2016).
[16]M. Harris, C. A. Hill, P. R. Tapster, and J. M. Vaughan, "Laser modes with helical wave fronts," Phys. Rev. A **49**, 3119–3122 (1994).
[17]A. Ghatak and K. Thyagarajan, *An Introduction to Fiber Optics* (Cambridge University Press, 1998).
[18]K. A. H. v Leeuwen and H. T. Nijnuis, "Measurement of higher-order mode attenuation in single-mode fibers: Effective cutoff wavelength," Opt. Lett. **9**, 252–254 (1984).
[19]A. Nicolas, L. Veissier, E. Giacobino, D. Maxein, and J. Laurat, "Quantum state tomography of orbital angular momentum photonic qubits via a projection-based technique," New J. Phys. **17**, 033037 (2015).
[20]P. M. Celliers, K. G. Estabrook, R. J. Wallace, J. E. Murray, L. B. D. Silva, B. J. MacGowan, B. M. V. Wonterghem, and K. R. Manes, "Spatial filter pinhole for high-energy pulsed lasers," Appl. Opt. **37**, 2371–2378 (1998).